Research Article ISSN 2641-4295

Food Science & Nutrition Research

Organ- and Harvest-Dependent Chemical Profiles and Antiproliferative Activity of Liriodendron chinense Extracts

Shaojie Qu[1], Guanyan Li[1], Yuanyuan Chen[1], Qing Mao[1], Xiaochen Yue[1]* and Wanxi Peng[2]*

[1]*College of Forestry, Henan Agricultural University, Zhengzhou, China.*

[2]*College of Forestry, Henan Agricultural University, Zhengzhou, China, College of chemistry and materials, Henan Agricultural University, Zhengzhou, China.*

***Correspondence:**
Wanxi Peng, College of Forestry and College of Chemistry and Materials, Henan Agricultural University, Zhengzhou, China.

Xiaochen Yue, College of Forestry, Henan Agricultural University, Zhengzhou, China

Received: 07 Oct 2026; **Accepted:** 11 Nov 2026; **Published:** 23 Nov 2026

Citation: Shaojie Qu, Guanyan Li, Yuanyuan Chen, et al. Organ- and Harvest-Dependent Chemical Profiles and Antiproliferative Activity of Liriodendron chinense Extracts. Food Sci Nutr Res. 2026; 9(4): 1-20.

ABSTRACT

Phytochemical and bioactivity studies of Liriodendron chinense remain insufficient. In this work, ethanol extracts of L. chinense were screened for antiproliferative activity against human bladder cancer 5637 cells to obtain the most potent sample and explore its chemical basis. The summer-harvested root extract exhibited the strongest inhibitory effect on cell viability, with approximately 83% inhibition after 48 h of incubation, and was therefore selected for phytochemical profiling. GC–MS and UPLC–Q-TOF–MS in positive-ion mode were combined to characterize its metabolites, covering volatile, semi-volatile and non-volatile constituents across a wide polarity range. Alkaloids, phenolics and terpenoids were the predominant secondary metabolite groups. All annotated compounds were further subjected to network pharmacology and molecular docking analyses to screen candidate bioactive constituents and predict their potential targets. Hub targets including PIK3CA, SRC and EGFR, as well as the PI3K–AKT and MAPK signaling pathways, were predicted to mediate the anti-proliferative activity. Collectively, this study identifies the summer-harvested root extract of L. chinense as a promising active sample against 5637 cells and provides testable hypotheses regarding its bioactive components and underlying molecular mechanisms.

Keywords

Liriodendron chinense, Harvesting period, Plant organ, Chemical profiling, Cell viability, Bladder cancer, Network pharmacology.

Research highlights

- FTIR, GC–MS, and UPLC–Q-TOF–MS provided complementary chemical coverage.
- Summer root extract reduced 5637-cell viability by approximately 83% at 48 h.
- PIK3CA, SRC, and EGFR emerged as putative hub targets in cancer pathways.

Introduction

Medicinal plants are important sources of structurally diverse natural products and have considerable value in the discovery of bioactive compounds and the development of plant-derived products [1,2].

Liriodendron chinense (Hemsl.) Sarg., a deciduous tree belonging to the Magnoliaceae family, is widely distributed in southern and central China and represents an important medicinal, ornamental, and forestry resource [3]. Different parts of this species have traditionally been used to manage inflammation, pain, and respiratory disorders [4]. Previous phytochemical investigations have shown that *L. chinense* contains structurally diverse constituents, including alkaloids, terpenoids, flavonoids, phenylpropanoids, steroids, and other phenolic compounds [5-7]. Several constituents reported in *L. chinense* or related species, such as liriodenine, lysicamine, berberine, 6-Shogaol, and dehydrocostus lactone, exhibit anti-inflammatory, cytotoxic,

or antitumor activities [8-12]. These findings indicate that *L. chinense* may have broader potential as a source of biologically active natural products.

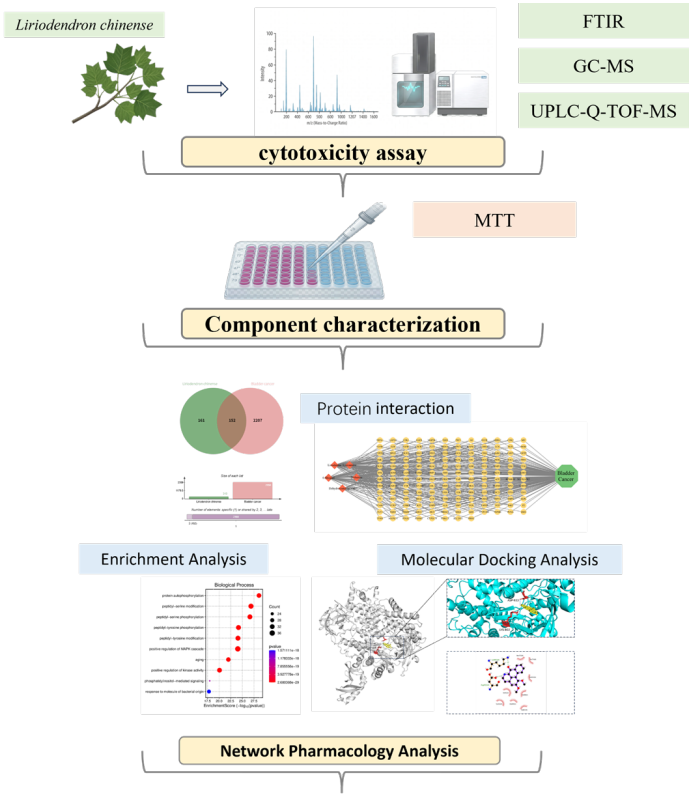

Because botanical extracts contain constituents with widely varying volatility, polarity, molecular mass, and ionization behavior, no single analytical technique can comprehensively characterize their chemical composition. Gas chromatography–mass spectrometry (GC–MS) is suitable for profiling volatile and semivolatile constituents [13,14]. Ultraperformance liquid chromatography coupled with quadrupole time-of-flight mass spectrometry (UPLC–Q-TOF–MS) provides complementary coverage of nonvolatile, thermolabile, and relatively polar constituents through accurate-mass measurement and MS/MS fragmentation analysis [15]. The combined application of these analytical platforms is therefore well suited to evaluating the chemical diversity of complex plant extracts.

Chemical characterization alone, however, cannot determine whether compositional variation is associated with differences in biological activity. Bladder cancer is a common urinary malignancy characterized by frequent recurrence and considerable biological heterogeneity [16]. The human bladder cancer 5637 cell line is widely used as an *in vitro* model for preliminary evaluation of cytotoxic and antiproliferative effects [17,18]. The cell-viability assay is used here primarily as a biological screening method to support resource evaluation rather than as evidence of clinical efficacy.

For complex botanical extracts, the biological effects observed *in vitro* may result from multiple constituents acting on interconnected targets and pathways. Network pharmacology, functional enrichment analysis, and molecular docking can predict associations between chemically annotated constituents and putative molecular targets and generate testable hypotheses regarding their potential biological actions [19]. These computational approaches are particularly useful for prioritizing candidate compounds and targets from complex chemical datasets.

In the present study, ethanol extracts were prepared from **L. chinense** and screened for antiproliferative activity against human bladder cancer 5637 cells via concentration–response MTT assays. The summer-harvested root extract with the most potent inhibitory effect was selected for chemical characterization. GC–MS and UPLC–Q-TOF–MS operated in positive-ion mode were combined to profile its volatile, semi-volatile and non-volatile metabolites. All tentatively annotated compounds from this active extract were further analyzed using network pharmacology, functional enrichment analysis, and molecular docking to screen candidate bioactive constituents, predict putative targets, and identify relevant signaling pathways. This integrated workflow aims to characterize the chemical profile of the active extract, explore its anti-bladder-cancer potential, and lay a foundation for follow-up mechanistic research.

Materials and Methods

Plant Material, Cell Line, and Reagents

L. chinense was collected from the Rock Garden Botanical Park in Zhumadian City, Henan Province, China (32.441289°N, 113.310397°E; altitude: 174 m). The human bladder carcinoma cell line 5637 was obtained from Wuhan Procell Life Science & Technology Co., Ltd. (Wuhan, China), with STR authentication completed by the supplier. Low-passage cells were used for all experiments, and PCR-based mycoplasma detection verified the absence of mycoplasma contamination before use. RPMI-1640 culture medium supplemented with 10% fetal bovine serum and 1% penicillin-streptomycin (100 U/mL penicillin and 100 µg/mL streptomycin) was also obtained from Wuhan Procell Life Science & Technology Co., Ltd. (Wuhan, China). Chromatographic-grade ethanol was purchased from Thermo Fisher Scientific (China). Phosphate-buffered saline (PBS) and trypsin were supplied by Servicebio (Wuhan, China). Beyotime Biotechnology (Shanghai, China) supplied the MTT Cell Proliferation and Cytotoxicity Assay Kit, while Sigma-Aldrich (St. Louis, MO, USA) provided dimethyl sulfoxide (DMSO).

Preparation of *Liriodendron chinense* Ethanol Extract

The dried material of *L. chinense* was pulverized and passed through a 40-mesh sieve. A total of 10.0 g of the powdered sample was placed in a flask, mixed with 300 mL of ethanol, and soaked at room temperature for 12 h and then extracted under reflux in a water bath at 78.5 °C for 5 h. The extract was filtered through qualitative filter paper and concentrated to approximately 10 mL by rotary evaporation at 45°C at an absolute pressure of 0.01 MPa. After the concentrate was filtered through a 0.22 µm membrane

filter, 1.0 mL of the concentrated extract was collected, dried in an oven at 30 °C, and further vacuum-freeze-dried to constant weight. The resulting product was temporarily stored at 0 °C in the dark.

Cell Viability Assay (MTT Method)

The MTT colorimetric assay was performed to evaluate the effects of six ethanol extracts of *Liriodendron chinense* on the viability of human bladder cancer 5637 cells. For each of the six extracts, 1.0 mL of the concentrated ethanol extract was collected and subjected to drying and subsequent vacuum freeze-drying. The resulting dried extract was reconstituted in DMSO to prepare a stock solution at a nominal concentration of 10 μg/mL. Before cell treatment, the stock solution was further diluted with complete culture medium to prepare the corresponding working solutions. The vehicle-control group received the corresponding DMSO concentration without extract.

Human bladder cancer 5637 cells in the logarithmic growth phase were detached by trypsin digestion, centrifuged, and resuspended in complete medium. The cell suspension was adjusted to a density of 5×10^4 cells/mL, and 100 μL of the suspension was seeded into each well of 96-well plates. Cells were incubated at 37 °C in a humidified atmosphere containing 5% CO_2 for 24 h to allow cell attachment. After attachment, the original culture medium was removed. For the treatment groups, 100 μL of the corresponding extract-containing working solution was added to each well. The vehicle-control group received 100 μL of complete medium containing the same final concentration of DMSO. Blank wells containing complete medium without cells were included for background correction. Six technical replicate wells were prepared for each condition, and all experiments were independently repeated at least three times.

Following treatment for 24 h, freshly prepared MTT solution (5 mg/mL) was added at 10 μL per well, and the plates were further incubated at 37 °C with 5% CO_2 for 4 h. The supernatant was then carefully removed, and 100 μL of DMSO was added to each well to dissolve the formed formazan crystals. The plates were incubated at 37 °C for approximately 15 min with gentle shaking. The absorbance was measured at 570 nm using a microplate reader.

The inhibition rate was calculated as:
Cell inhibition rate (%) = [1 − (OD_{570} of the experimental group / OD_{570} of the vehicle-control group)] × 100%.

The six extracts were initially screened under the same MTT treatment conditions to identify the extract exhibiting the strongest inhibitory effect on 5637-cell viability. The summer-root extract (S-R) showed the highest inhibitory activity and was therefore selected for subsequent concentration-response and time-course experiments. For the concentration-response experiment, the S-R working solution was diluted with complete medium at volume ratios of 1:8, 1:4, 1:2, 1:1, and 2:1. Following identification of the most effective treatment proportion, the corresponding condition was used for the subsequent time-course experiment. Cells were treated for 6, 12, 18, 24, 30, 36, 42, and 48 h, respectively. Cell viability and inhibition rate were determined using the same MTT procedure described above.

GC–MS Analysis and UPLC–Q-TOF–MS Analysis

GC–MS: Analysis was performed on an Agilent 7890A−5975C system (Agilent Technologies, USA) equipped with an HP-5MS capillary column (30 m × 0.25 mm, i.d., 0.25 μm film thickness). Helium was used as the carrier gas at a flow rate of 1 mL/min. The injector temperature was set at 250 °C and the ion-source temperature was maintained at 230 °C. The oven temperature program was as follows: the initial temperature was maintained at 60 °C for 2 min, increased to 280 °C at 10 °C/min, and maintained at 280 °C for 10 min. The injection volume was 1 μL with a split ratio of 10:1. Mass spectra were acquired in electron impact (EI) mode at 70 eV over a scan range of 50−500 m/z. Prior to injection, dried ethanol extract was dissolved in chromatographic-grade absolute ethanol and filtered through a 0.22 μm organic membrane filter. Solvent blank and quality-control samples were analyzed alongside test samples to exclude contamination and instrument drift. Compounds were tentatively annotated by comparing their mass spectra with the NIST 14 library with a match threshold ≥850. Retention indices were calculated using a series of n-alkanes for further compound validation. Peak-area normalization was applied for relative quantitative comparison. Compounds were tentatively annotated by integrating NIST library spectral matching and experimentally determined retention indices calculated from n-alkanes. Due to the absence of authentic reference standards, definitive compound confirmation was not performed in the present work.

UPLC–Q-TOF–MS: A Waters ACQUITY UPLC system connected to a Xevo G2-XS QTOF mass spectrometer (Waters, USA) was used for the analysis. Chromatographic separation was achieved on an ACQUITY UPLC BEH C18 column (100 mm × 2.1 mm, 1.7 μm) using a mobile phase consisting of 0.1% formic acid in water (A) and acetonitrile (B). The gradient schedule included: 0 to 5 min at 5−20% B; 5 to 15 min at 20−50% B; 15 to 25 min at 50−80% B; 25 to 30 min at 80−95% B; 30 to 32 min at 95−5% B, followed by an 8-min column re-equilibration step before the next injection, giving a total run time of 40 min. The flow rate was 0.3 mL/min, the column temperature was maintained at 35 °C, and the injection volume was 5 μL.

Network Pharmacology Analysis

Prediction of Compound-Related Targets

The canonical SMILES strings of compounds tentatively annotated by GC-MS and UPLC-Q-TOF-MS after ADME filtering (detailed criteria described in Results section) were retrieved from the PubChem database (https://pubchem.ncbi.nlm.nih.gov/). No compounds with known pharmacological activities were manually supplemented in this work to avoid confirmation bias and guarantee analytical reproducibility.

Potential protein targets were predicted using the STITCH 5.0 database (http://stitch.embl.de/) and the SwissTargetPrediction platform (http://www.swisstargetprediction.ch/), with the species

restricted to Homo sapiens. Duplicate targets were removed to obtain a non-redundant set of compound-related targets. In the STITCH 5.0 database, target screening was performed using the confidence score (combined score) as the criterion, and only targets with medium or higher confidence levels (combined score ≥ 0.400) were retained. For compounds with relatively few predicted targets from SwissTargetPrediction, STITCH 5.0 results were used as supplementary information, provided that the included targets met the predefined confidence threshold in at least one database.

All predicted targets were standardized using the UniProt database (https://www.uniprot.org/), with species restricted to Homo sapiens, and were uniformly converted into official gene symbols. After removing duplicates, non-human targets, and entries that could not be standardized, a non-redundant set of compound-related targets was obtained for subsequent intersection analysis and network construction.

Identification of Bladder Cancer-Related Targets

Bladder cancer-associated target genes were collected from the GeneCards (https://www.genecards.org/; accessed: Month Day, Year) and OMIM (https://omim.org/) databases using the keyword "bladder cancer". For GeneCards, targets were retained with a relevance score ≥ 5 as the filtering threshold to exclude weakly-associated genes.

Construction of Protein–Protein Interaction Network and Core Target Screening

An online bioinformatics platform (http://www.bioinformatics.com.cn/) was used to generate a Venn diagram to identify and display the intersection of compound-associated targets and bladder cancer-associated targets. The overlapping targets were imported into the STRING database (https://string-db.org/; version 12.0), with organism restricted to *Homo sapiens*. All available interaction-source evidence including text-mining, experimental evidence, database evidence, co-expression, co-occurrence, gene neighborhood and gene fusion were activated. The interaction score threshold was set to 0.9 for highest confidence. The exported PPI network data were further analyzed in Cytoscape software. Topological parameters including degree centrality (DC), betweenness centrality (BC), and closeness centrality (CC) were calculated via the CytoNCA plugin. Hub targets were defined as genes whose DC, BC and CC values were all higher than their respective median values calculated from the whole PPI network.

Network Construction

A "compound–target–disease" interaction network was constructed and visualized in Cytoscape to illustrate the predicted associations among candidate compounds, putative protein targets, and bladder cancer.

Functional Enrichment Analysis

Gene Ontology (GO) functional annotation and KEGG pathway enrichment analyses were performed on the intersecting target genes using an online bioinformatics platform (http://www.bioinformatics.com.cn/). The organism was set to *Homo sapiens*. The hypergeometric test was adopted as the enrichment algorithm, and the whole human genome served as the background gene set. The Benjamini-Hochberg method was applied for multiple-testing correction. Terms with adjusted P-value < 0.05 and a minimum gene count ≥ 3 were regarded as significantly enriched entries. Significantly enriched biological processes, cellular components, molecular functions, and signaling pathways were visualized accordingly.

Molecular Docking Analysis

The three-dimensional crystal structures of putative hub proteins (PIK3CA, SRC, and EGFR) were retrieved from the Protein Data Bank (PDB; https://www.rcsb.org/). The co-crystallized ligands were extracted from the crystal structures. Prior to formal molecular docking, redocking of the native co-crystallized ligand was performed for each target protein to evaluate the reliability of the docking parameter settings.Compound structures of candidate molecules were obtained from PubChem, followed by energy minimization using ChemDraw and Chem3D. Molecular docking simulations were carried out with AutoDock 4.2. Docking poses were ranked by predicted binding free energies calculated by AutoDock 4.2. The representative pose with the lowest predicted binding free energy within the most populated cluster was selected as the optimal binding mode. Three-dimensional docking interactions were visualized using PyMOL 3.1.6.1, and two-dimensional interaction diagrams were generated by LigPlot+ 2.3.1.

Results and Analysis

Anti-proliferative Effects

The MTT assay was first used to screen the effects of the six *L. chinense* ethanol extracts on the viability of human bladder cancer 5637 cells. The six extracts, including summer leaf, summer stem, summer root, autumn leaf, autumn stem, and autumn root extracts, were prepared from 1.0 mL of the corresponding concentrated ethanol extract, freeze-dried, and reconstituted in DMSO to obtain stock solutions at a nominal concentration of 10 μg/mL. The stock solutions were subsequently diluted with complete medium before cell treatment. All six extracts were evaluated under the same MTT assay conditions.

Two-way factorial ANOVA revealed a statistically significant main effect of plant organ on the inhibition of 5637-cell viability ($F(2, 12) = 23.59$, $p < 0.001$), whereas the main effect of harvesting period was not statistically significant ($F(1, 12) = 2.22$, $p = 0.161$). The interaction between plant organ and harvesting period was also not statistically significant ($F(2, 12) = 1.34$, $p = 0.297$). Bonferroni-adjusted comparisons showed that the summer-root extract produced the highest inhibition rate, reaching 70.20% ± 6.29%. The inhibition rates of the other extracts were 63.29% ± 1.45% for autumn root, 57.38% ± 5.06% for summer leaf, 53.64% ± 5.84% for autumn leaf, 50.18% ± 3.63% for autumn stem, and 48.83% ± 1.53% for summer stem. Overall, the root extracts showed relatively stronger inhibitory activity than the stem and leaf extracts. Based on its highest inhibitory activity in the initial screening, the summer-root extract was selected for subsequent

concentration-response and time-course experiments.

The concentration-response effect of the summer-root extract on 5637-cell viability was subsequently evaluated after 24 h of treatment. Five treatment proportions of the summer-root working solution to complete medium were tested: 1:8, 1:4, 1:2, 1:1, and 2:1. One-way ANOVA demonstrated significant differences in inhibition rates among the five treatment groups ($F(4, 10) = 97.48$, $p < 0.0001$). The inhibition rate generally increased with increasing proportions of the extract-containing working solution. The inhibition rates were 20.95% ± 5.41% at 1:8, 47.39% ± 2.47% at 1:4, 58.03% ± 2.17% at 1:2, 63.57% ± 2.24% at 1:1, and 65.89% ± 2.52% at 2:1. Thus, increasing the treatment proportion from 1:8 to 1:4 produced a pronounced increase in inhibition, followed by a further but smaller increase at higher treatment proportions. The 2:1 condition showed the highest inhibition rate and was therefore selected for the subsequent time-course experiment.

The time-dependent inhibitory effect of the summer-root extract was then evaluated using the 2:1 extract-working-solution-to-medium proportion. Cells were treated for 6, 12, 18, 24, 30, 36, 42, and 48 h. One-way ANOVA showed significant differences in inhibition rates among the different treatment durations ($F(7, 16) = 75.23$, $p < 0.0001$). The inhibition rate increased from 27.07% ± 3.66% at 6 h to 60.67% ± 1.64% at 12 h, 71.35% ± 5.79% at 18 h, and 78.40% ± 2.81% at 24 h. A slight decrease was observed at 30 h, with an inhibition rate of 74.53% ± 1.61%. Thereafter, the inhibitory effect remained relatively stable between 36 and 42 h, and the highest inhibition rate, 83.74% ± 5.72%, was observed after 48 h of treatment.

Taken together, the six *L. chinense* ethanol extracts exhibited different inhibitory effects on the viability of 5637 cells under the tested conditions. Among the six extracts, the summer-root extract showed the strongest inhibitory activity and was therefore selected for further evaluation. The summer-root extract exhibited a concentration-dependent inhibitory pattern across the tested treatment proportions and a generally time-dependent increase in inhibition, with the maximum inhibition rate of 83.74% ± 5.72% observed after 48 h at the 2:1 treatment proportion. Because the MTT assay primarily reflects cellular metabolic activity, these findings demonstrate inhibition of MTT-measured cell viability rather than definitively establishing cell death or a specific cytotoxic mechanism.

GC-MS analysis and UPLC-Q-TOF-MS Analysis

GC–MS Analysis

GC–MS was used to profile the volatile and semi-volatile constituents in the summer root ethanol extract. A total of 12 compounds were tentatively annotated by matching mass spectra with the library and verifying with experimentally determined retention indices, and their relative contents were calculated by peak area normalization (Figure 2). The annotated compounds were mainly divided into terpenoids, alcohols, amides, phenols and aliphatic hydrocarbons, among which sesquiterpenoids and their oxygenated derivatives dominated the volatile profile. The most abundant constituent was Azulene[4,5-b]furan-2(3H)-one, decahydro-3,6,9-tris(methylene)-,[3aS-(3a.alpha.,6a.alpha.,9a.alpha.,9b.beta.)]-, accounting for 63.73% of the total normalized peak area. The second most abundant component was 2-Naphthalenemethanol, decahydro-. alpha.,. alpha.,4a-trimethyl-8-methylene-, [2R-(2.alpha.,4a.alpha.,8a.beta.)]- (12.52%), followed by 13-Docosenamide, (Z)- (6.56%) and 2(3H)-Benzofuranone, 6-ethenylhexahydro-6-methyl-3-methylene-7-(1-methylethenyl)-, [3aS-(3a.alpha.,6.alpha.,7.beta.,7a.beta.)]- (4.87%).

Overall, GC–MS mainly covered the low-polarity, thermally stable volatile and semi-volatile fractions of the summer root extract, and sesquiterpene lactones represented the most prominent chemical class in this fraction. Among the annotated constituents, Dehydrocostus lactone, as a typical bioactive sesquiterpene

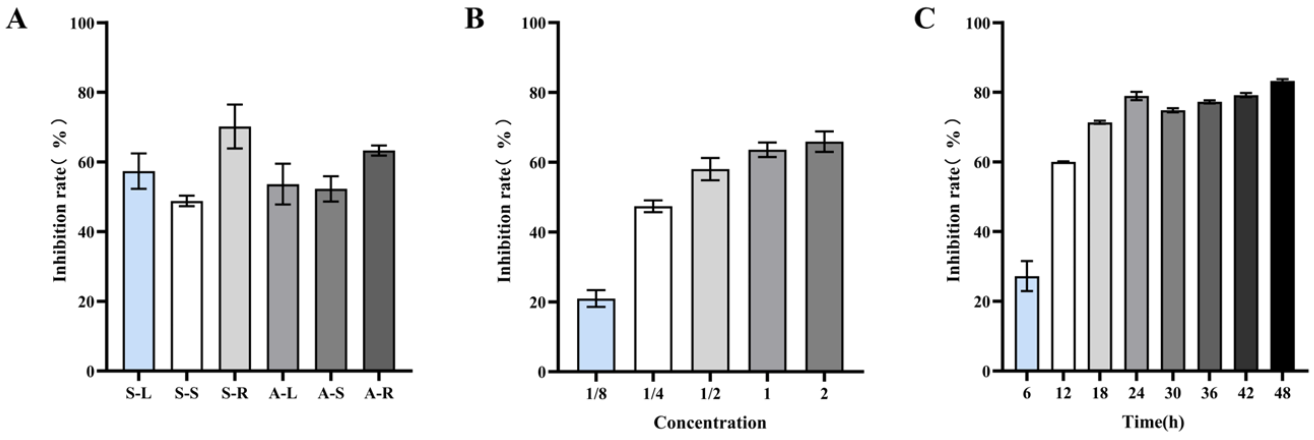

Figure 1: Effects of L. chinense ethanol extracts on MTT-derived inhibition of 5637-cell viability:
(A) Comparison of summer and autumn leaf, stem, and root extracts under the initial screening conditions; (B) concentration-response relationship of the summer-root extract after 24 h of treatment; and (C) time-course response to the summer-root extract at an extract-to-medium ratio of 2:1. Data are presented as mean ± SD from three independent experiments, with six technical replicate wells per condition in each experiment.

lactone, provides an important volatile active candidate for the summer root extract.

UPLC–Q-TOF–MS Analysis

To further characterize medium-polarity and high-polarity non-volatile constituents, UPLC–Q-TOF–MS analysis was performed in electrospray positive ionization mode (ESI^+).

A total of 275 molecular features were tentatively annotated in the summer root extract, covering diverse chemical classes including alkaloids, phenolics, terpenoids, lipids, glycosides and other secondary metabolites. Alkaloids and terpenoids were the predominant secondary metabolite groups. Representative annotated compounds included a series of isoquinoline alkaloids such as berberine, liriodenine, lysicamine, lanuginosine and nandazurine, various sesquiterpenes, diterpenes and triterpenes, as well as phenolic compounds such as 6-shogaol.

These annotated compounds constituted the chemical dataset of the summer root extract, which was imported into the subsequent network pharmacology workflow to screen potential antiproliferative active constituents against bladder cancer.

The combined application of GC–MS and UPLC–Q-TOF–MS (ESI^+) provided complementary chemical coverage for the summer root extract, jointly depicting its multi-polarity chemical profile. GC–MS revealed that sesquiterpene lactones dominated the volatile fraction, with dehydrocostus lactone accounting for more than 60% of the total volatile peak area. UPLC–Q-TOF–MS in positive ionization mode further expanded the chemical coverage to medium- and high-polarity constituents and identified abundant alkaloids, phenolics and terpenoids. This multi-platform characterization strategy comprehensively reflected the chemical complexity of the active extract.The annotated constituents were subsequently subjected to network pharmacology screening to prioritize compounds with potential anti-bladder-cancer activity.

Network Pharmacology Analysis

Target Screening and Network Construction

To elucidate candidate constituents potentially associated with the observed effect of the ethanol extract of *L. chinense* on 5637-cell viability and their molecular basis of action, candidate compounds were first screened by integrating tentative chemical annotation results, ADME properties, and evidence from the literature. The candidate compounds were derived from the GC–MS and UPLC–Q-TOF–MS results and were evaluated for ADME-related and drug-likeness properties using the SwissADME platform.The screening criteria were as follows: molecular weight (MW) between 180 and 500; topological polar surface area (TPSA) between 20 and 140 Å², with TPSA < 140 Å² generally indicating favorable intestinal absorption potential; high predicted gastrointestinal absorption and no predicted P-glycoprotein substrate status; at least three "Yes" results in the drug-likeness assessment; and no PAINS alerts. Blood-brain barrier permeability (BBB permeant) was recorded as a pharmacokinetic characteristic, with "Yes" indicating potential entry into the central nervous system and "No" indicating limited likelihood of acting on brain targets. However, as this study focused on bladder cancer, BBB permeability was not used as an exclusion criterion. Ultimately, five representative compounds that met the above ADME screening criteria were selected [20,21].

Among compounds that met the predicted ADME criteria,

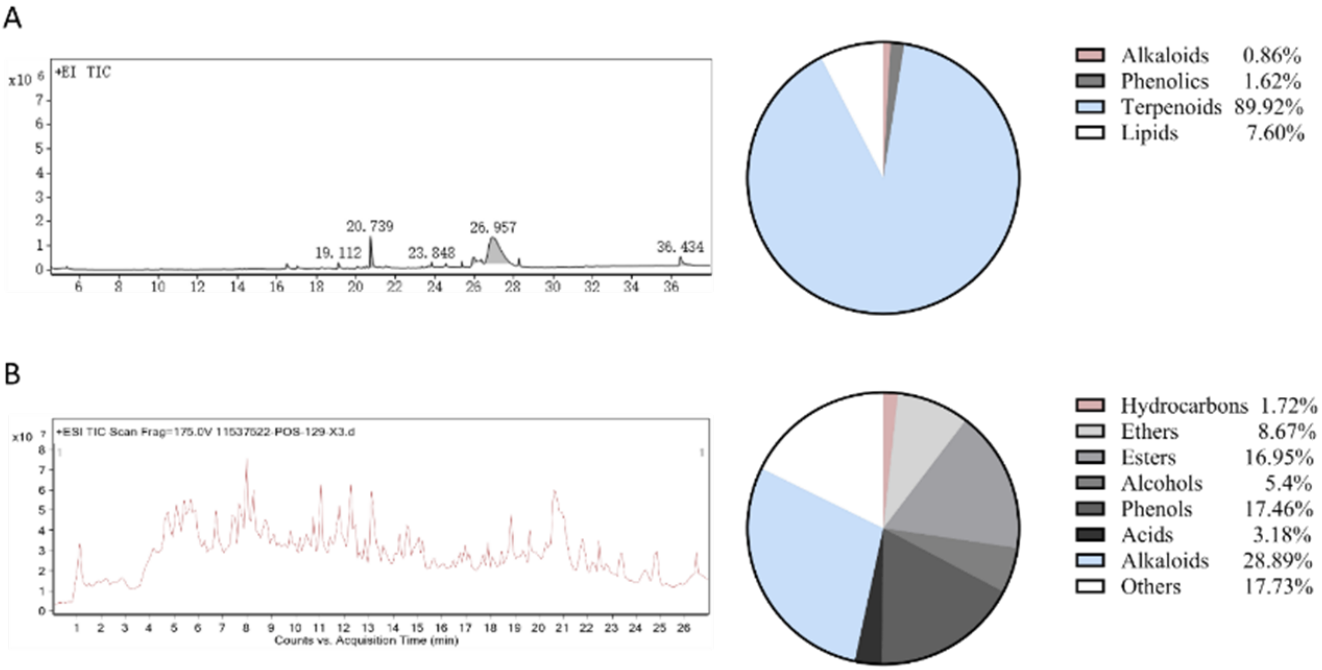

Figure 2: A: Total ion chromatogram (TIC) of summer root obtained by GC–MS.
B: Total ion chromatogram (TIC) of summer root obtained by UPLC–Q-TOF–MS

published evidence retrieved through Web of Science and CNKI searches was further considered. Priority was given to compounds that had been reported to possess antitumor, antiproliferative, proapoptotic, or cancer-related signaling pathway-modulating activities and that were tentatively annotated in the GC–MS or UPLC–Q-TOF–MS datasets. This screening strategy was not based solely on literature reports or single peak-area abundance, but instead integrated three aspects: chemical detectability, pharmacokinetic feasibility, and evidence of known bioactivity, to prioritize compounds for subsequent target prediction and network construction. Based on these criteria, five candidate constituents were prioritized, including lysicamine, berberine, 6-shogaol, liriodenine, and dehydrocostus lactone.

The STITCH and SwissTargetPrediction databases were used to predict potential targets for these five compounds. After integrating the data and removing duplicates, 313 potential compound-associated targets were predicted. In parallel, 2359 bladder cancer-associated targets were retrieved from the GeneCards and OMIM databases using "bladder cancer" as the keyword. An intersection analysis of compound- and disease-related targets identified 152 overlapping genes, which were retained as candidate targets for subsequent analysis. It should be noted that the above results were primarily based on database predictions and molecular similarity inferences and may therefore include false positives and false negatives. Accordingly, these targets were regarded in the present study as candidate targets rather than experimentally validated direct pharmacological targets. To restrict the PPI analysis to high-confidence reported interactions, a subsequent PPI analysis was performed on high-confidence interactions from the STRING database, applying a combined score threshold of > 0.900 in network analysis.

The STRING-derived PPI network of the 152 intersecting targets was imported into Cytoscape for topological analysis to further identify key regulatory nodes. Using the CytoNCA plugin, a three-step filtering process based on median values of degree centrality (DC), betweenness centrality (BC), and closeness centrality (CC) was applied. This analysis ultimately identified three targets—PIK3CA, SRC, and EGFR—as putative hub nodes within the network. From a biological functional perspective, PIK3CA is a key upstream component of the PI3K/AKT pathway and directly participates in regulating cell proliferation and survival. SRC is a non-receptor tyrosine kinase closely associated with tumor migration, invasion, and proliferative signaling [22]. EGFR, a receptor tyrosine kinase frequently implicated in bladder cancer, can activate oncogenic pathways such as PI3K/AKT and MAPK [23]. Therefore, these three targets ranked as putative hubs within the constructed PPI network; however, their network centrality does not establish causal roles in the response of 5637 cells to the extract.

A "compound–target–disease" interaction network was subsequently constructed in Cytoscape to visualize relationships among the five candidate compounds, the intersecting targets, and bladder cancer. In this network, nodes represent compounds, genes, and diseases, while edges denote database-predicted or previously reported associations. The network predicted that different compounds may be associated with distinct cancer-related targets. For example, both berberine and liriodenine were associated

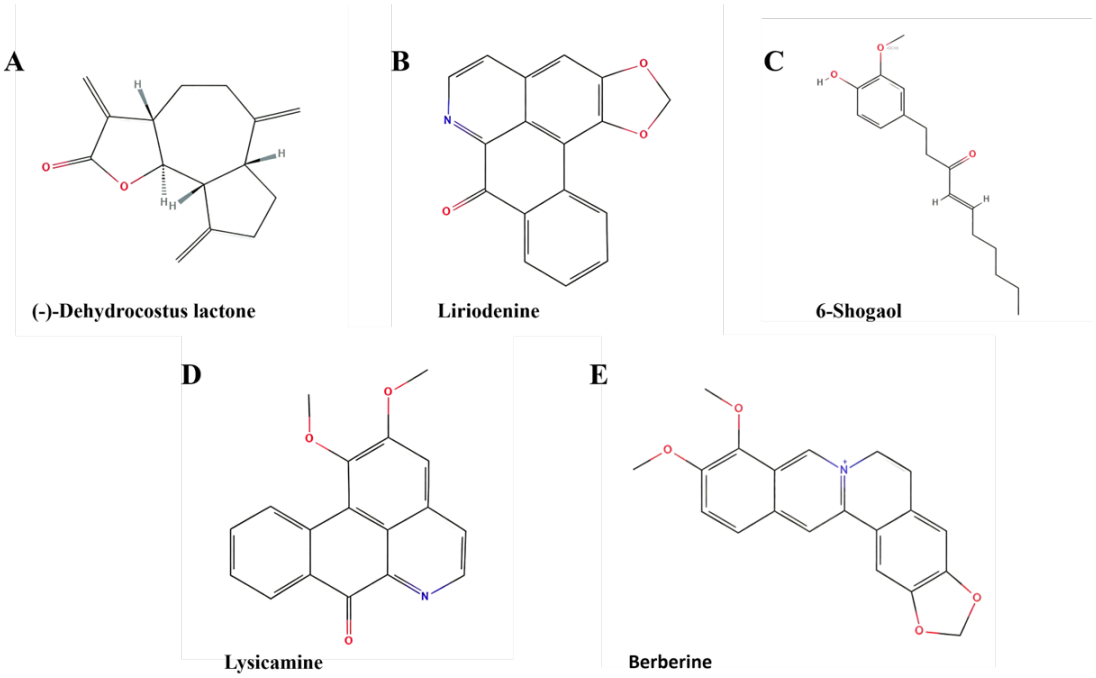

Figure 3: Chemical structures of the five candidate compounds: (A) (−)-dehydrocostus lactone, tentatively annotated by GC–MS; and (B–E) liriodenine, 6-shogaol, lysicamine, and berberine, respectively, tentatively annotated by UPLC–Q-TOF–MS.

with PIK3CA, suggesting a possible association with PI3K/AKT signaling; however, the direction and cellular consequences of these associations were not determined. Dehydrocostus lactone was associated with targets such as SRC and EGFR, suggesting potential associations with tyrosine kinase-related MAPK and PI3K signaling. Although 6-shogaol was predicted to have fewer targets, it retained a predicted association with PIK3CA-related pathways.

Overall, the network analysis suggested that the five candidate compounds may be associated with multiple predicted targets and generated testable mechanistic hypotheses. Specifically, PIK3CA, SRC, and EGFR emerged as putative network hubs associated with the PI3K/AKT and MAPK pathways; however, compound–target binding, pathway inhibition, and effects on cell proliferation were not experimentally demonstrated.

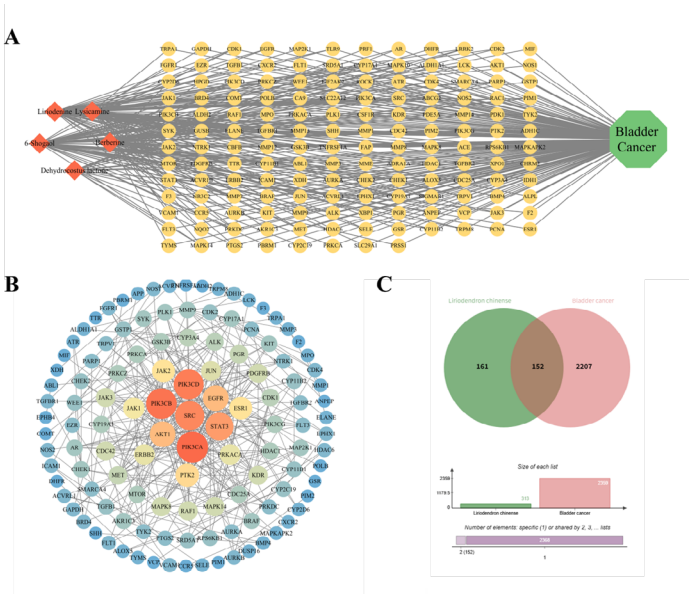

Figure 4: Network pharmacology analysis of five candidate compounds tentatively annotated in the *L. chinense* ethanol extract. (A) Compound–target–disease network showing predicted associations among the five candidate compounds, 152 overlapping targets, and bladder cancer; red diamonds, yellow circles, and the green octagon represent candidate compounds, overlapping targets, and bladder cancer, respectively. (B) STRING-derived protein–protein interaction network of the 152 overlapping targets; node size and color intensity represent relative topological importance, with PIK3CA, SRC, and EGFR identified as the final putative hubs. (C) Venn diagram showing the intersection between 313 predicted compound-associated targets and 2,359 bladder cancer-associated targets, yielding 152 overlapping targets.

Functional Enrichment Analysis

To gain a deeper understanding of the biological roles and signaling pathways associated with the 152 overlapping candidate genes, KEGG pathway enrichment analysis was performed on these genes using an online bioinformatics platform. KEGG pathway analysis returned 28 cancer-related pathways that met the specified enrichment threshold. Among these, "Pathways in cancer" (hsa05200) and "Proteoglycans in cancer" (hsa05205) exhibited the highest enrichment scores, with $-\log_{10}(P)$ values of 34.21 and 18.42, respectively. These pathways are closely associated with tumor progression, proliferation, cell survival, migration and extracellular matrix remodeling, indicating that the candidate overlapping genes were enriched in several oncogenic signaling pathways. However, enrichment analysis does not establish pathway activation, inhibition, directionality, or modulation by the extract.

GO enrichment analysis ($P < 0.05$, FDR < 0.01) further revealed that the intersecting targets were significantly enriched across biological processes (BP), cellular components (CC), and molecular functions (MF). In the BP category, the targets were primarily associated with protein autophosphorylation (GO:0046777), peptidyl-serine modification (GO:0018108), and peptidyl-serine phosphorylation (GO:0006468), indicating enrichment of candidate genes annotated to kinase-related biological processes. In the CC category, enrichment was mainly observed in membrane rafts (GO:0045121) and membrane microdomains (GO:0098857), indicating enrichment of gene products annotated to specialized membrane regions. In the MF category, the dominant terms included transmembrane receptor protein kinase activity (GO:0004713) and protein serine/threonine kinase activity (GO:0004674), indicating enrichment of kinase-related molecular functions among the candidate genes.

The enrichment results showed an overrepresentation of kinase-related terms and signaling pathways, particularly those associated with the PI3K/AKT and MAPK cascades, which regulate cancer cell proliferation and survival. The enriched GO terms independently included membrane rafts and microdomains, protein phosphorylation processes, and receptor and serine/threonine kinase activities; however, enrichment analysis cannot establish a sequential functional cascade among these terms. These GO results were conceptually consistent with KEGG enrichment in PI3K/AKT-, MAPK-, and cancer-related pathways, supporting the hypothesis that candidate constituents may be associated with membrane receptor kinase signaling and downstream phosphorylation pathways. These findings provide a hypothesis-generating overview of pathways potentially associated with the observed reduction in 5637-cell viability.

Overall, the enrichment analysis generated a network-based hypothesis linking the five candidate compounds to putative hubs such as EGFR, SRC, and PIK3CA, as well as to kinase-related pathways, including PI3K/AKT and MAPK; these associations remain experimentally unvalidated. The time-associated reduction in the MTT signal does not independently validate these predicted molecular associations. Moreover, the concurrent enrichment of multiple pathways reflects overlap between the candidate gene set and several annotation categories, but does not establish coordinated multitarget regulation by the extract.

Molecular Docking Analysis

To assess the potential structural compatibility between the

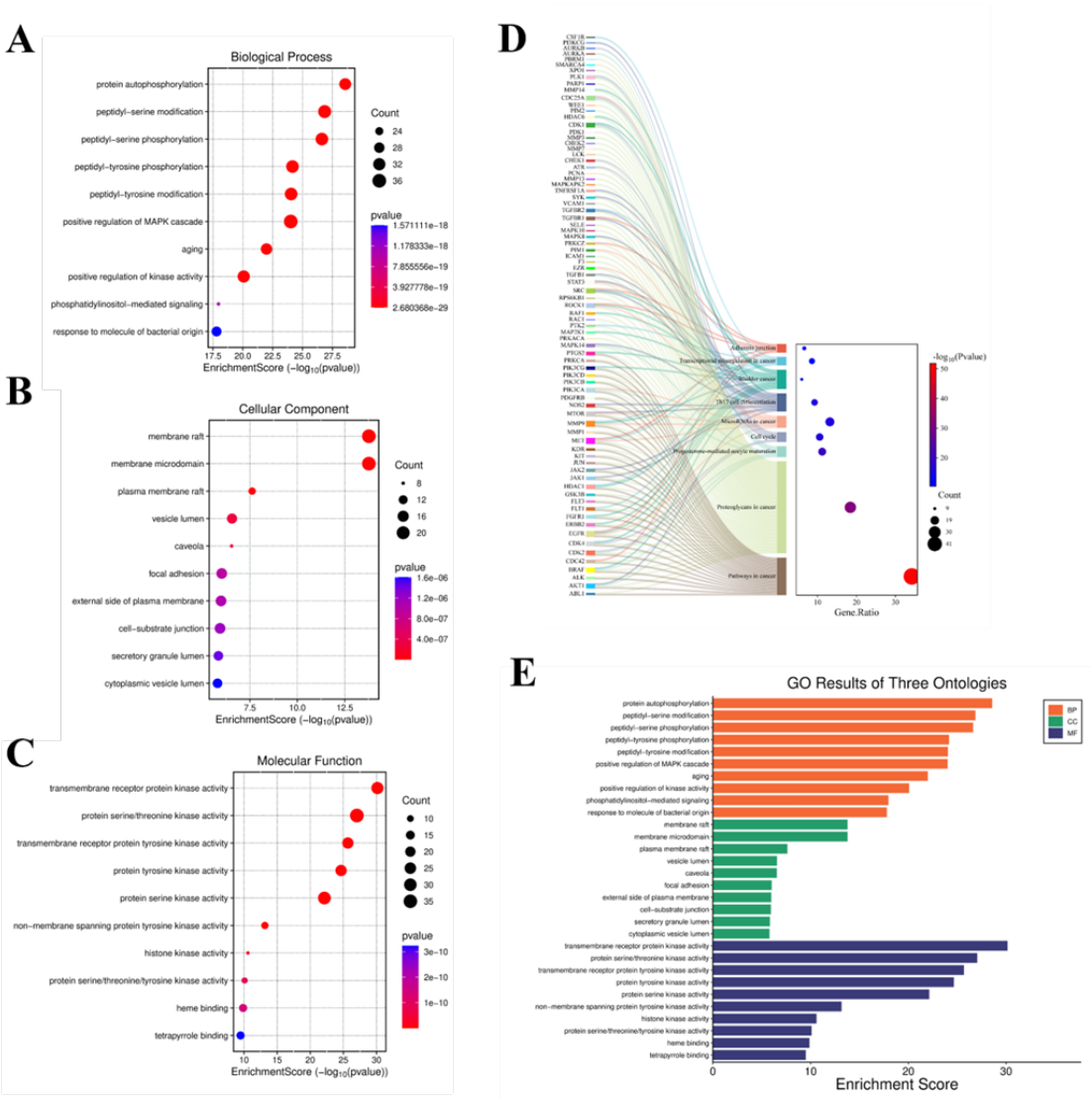

Figure 5: Functional enrichment analysis of the 152 candidate overlapping genes: bubble plots of enriched Gene Ontology (GO) terms in the categories of (A) biological process, (B) cellular component, and (C) molecular function; (D) Kyoto Encyclopedia of Genes and Genomes (KEGG) pathway enrichment visualized using a gene–pathway Sankey diagram and bubble plot; and (E) bar-chart summary of the enriched GO terms across the three ontology categories.

five candidate compounds—lysicamine, berberine, 6-shogaol, liriodenine, and dehydrocostus lactone—and the three putative hub proteins PIK3CA, SRC, and EGFR, a total of 15 compound–protein docking systems were evaluated. Crystal structures of the target proteins were retrieved from the RCSB Protein Data Bank. Water molecules and co-crystallized ligands were removed, after which polar hydrogen atoms were added, and Gasteiger charges were assigned. Ligand structures were retrieved from PubChem and energy-minimized using Chem3D. Protein and ligand preparation were performed using AutoDockTools 1.5.7, and docking calculations were conducted using AutoDock 4.2. The grid box was centered on the experimentally defined binding pocket of each protein with a grid spacing of 0.375 Å. Multiple independent docking runs were performed for each compound–protein system, and the pose with the lowest predicted binding energy within a well-populated cluster was selected as the representative binding mode. Three-dimensional binding poses were visualized using PyMOL 3.1.6.1, and two-dimensional interaction diagrams were generated using LigPlot+ 2.3.1.

The predicted docking energies for the 15 compound–protein pairs ranged from −3.02 ± 0.18 to −9.50 ± 0.41 kcal/mol. Thirteen of the 15 pairs yielded predicted energies more negative than −5 kcal/mol, indicating comparatively favorable docking scores within the applied computational protocol; however, these values do not independently demonstrate binding affinity or complex stability. Among the three putative targets, PIK3CA showed the most favorable overall docking scores: lysicamine, −8.20 ± 0.35 kcal/mol; berberine, −7.90 ± 0.33 kcal/mol; 6-shogaol, −6.00 ± 0.28 kcal/mol; liriodenine, −9.50 ± 0.41 kcal/mol; and dehydrocostus

lactone, −9.10 ± 0.38 kcal/mol. The predicted poses suggested that hydrophobic contacts, aromatic interactions, hydrogen bonding, and van der Waals interactions may contribute to the comparatively favorable scores of liriodenine and dehydrocostus lactone with PIK3CA. By contrast, 6-shogaol produced less favorable docking scores with EGFR (−3.02 ± 0.18 kcal/mol) and SRC (−3.32 ± 0.19 kcal/mol). Overall, the docking results prioritize selected compound–protein pairs for experimental evaluation but do not confirm direct binding or target modulation.

Among the five candidate compounds, PIK3CA generally yielded more favorable predicted docking energies than those for EGFR and SRC. Among the 15 evaluated combinations, PIK3CA–liriodenine and PIK3CA–dehydrocostus lactone produced the most favorable docking scores and were therefore prioritized for further experimental investigation. Although 6-shogaol showed comparatively weak docking scores with EGFR and SRC, its predicted interaction with PIK3CA was more favorable within the applied docking protocol. However, these score differences do not establish statistically significant binding, biological target selectivity, or direct compound–protein interactions.

From a biological perspective, PIK3CA encodes the p110α catalytic subunit of class IA phosphoinositide 3-kinase and contributes to the regulation of cancer cell proliferation, survival, and metabolism through the PI3K/AKT signaling pathway [24]. The comparatively favorable docking scores of the candidate compounds toward PIK3CA suggest that these compounds may interact with this target; however, the docking results do not demonstrate inhibition of PI3K/AKT signaling, reduced AKT phosphorylation, or suppression of 5637-cell proliferation [25]. The computational prioritization of PIK3CA was aligned with the network pharmacology and functional enrichment results, although these analyses are not independent experimental evidence of pathway modulation.

Overall, the compounds showed different predicted docking scores across the three putative targets, with generally more favorable scores for PIK3CA. This pattern was conceptually consistent with the enrichment of kinase-related terms and pathways. Nevertheless, molecular docking provides only predictions of structural compatibility and does not establish direct binding, target selectivity, target engagement, or biological activity. Biophysical binding assays, target-engagement studies, and measurements of PI3K/AKT pathway activity and AKT phosphorylation are therefore required to determine the biological relevance of these predicted interactions.

Discussion

Candidate bioactive constituents provide a possible chemical basis for the cellular response

The GC-MS and UPLC–Q-TOF–MS analysis provided a broader chemical perspective and enabled tentative annotation of several compounds with previously reported biological activities. Five constituents—berberine, lysicamine, 6-shogaol, liriodenine, and dehydrocostus lactone—were prioritized because they were chemically annotated in the investigated extract and had reported antitumor, antiproliferative, proapoptotic, or cancer-related activities. Their presence in the summer-root extract provides a reasonable starting point for interpreting its relatively strong effect on 5637-cell viability.

Among these candidates, berberine is particularly relevant to the present model because its anticancer activity has been experimentally investigated in bladder cancer cells, including the 5637 cell line. Berberine has been reported to inhibit proliferation, migration, invasion, and cell-cycle progression in T24 and 5637 cells while promoting apoptosis and suppressing HER2/PI3K/AKT signaling [26]. In addition, studies in other cancer models have associated berberine with inhibition of PI3K/AKT signaling, AMPK-related regulation, apoptosis, autophagy, and oxidative-stress responses [27,28]. These findings are of particular interest because PI3K/AKT signaling also emerged from the network analysis in the present study, providing a degree of biological convergence between the chemical annotation and the computational prediction. 6-Shogaol provides another potential link between the chemical and computational findings. Previous studies have associated 6-shogaol with inhibition of cancer-cell growth through several interconnected processes, including ROS generation, apoptosis, autophagy, and suppression of AKT/mTOR signaling [29]. Experimental work in cervical cancer has further demonstrated involvement of the PI3K/Akt/mTOR axis in its antitumor effects [30]. Therefore, although the present study does not directly demonstrate the action of 6-shogaol in 5637 cells, its tentative detection provides a plausible chemical candidate that is consistent with the broader signaling pattern identified by network analysis. Dehydrocostus lactone may be particularly important in interpreting the PI3K/AKT and MAPK-related findings. Experimental studies in several cancer models have shown that this sesquiterpene lactone can inhibit proliferation, induce apoptosis, and interfere with PI3K/AKT signaling. In gastric cancer, for example, dehydrocostus lactone was reported to inhibit proliferation and epithelial–mesenchymal transition through PI3K/AKT and ERK/MAPK signaling, while studies in other tumor models have likewise linked its activity to inhibition of AKT phosphorylation and induction of apoptosis [31]. This overlap is notable because both PI3K/AKT- and MAPK-related signaling emerged among the enriched pathways in the present network analysis. Liriodenine and lysicamine provide additional, although less directly established, candidates. Liriodenine has been reported to inhibit cancer-cell proliferation and induce cell-cycle arrest and apoptosis in lung cancer cells, while lysicamine and related oxoaporphine alkaloids have shown cytotoxic activity in several experimental cancer models [32]. Their tentative annotation in the summer-root extract therefore broadens the range of possible bioactive constituents beyond the better-characterized berberine and dehydrocostus lactone. Nevertheless, evidence for their specific activity against bladder cancer remains limited compared with that for berberine [33]. Taken together, these observations suggest that the activity of the summer-root extract may result from the combined contribution of several structurally different constituents rather than from a single dominant compound. Such

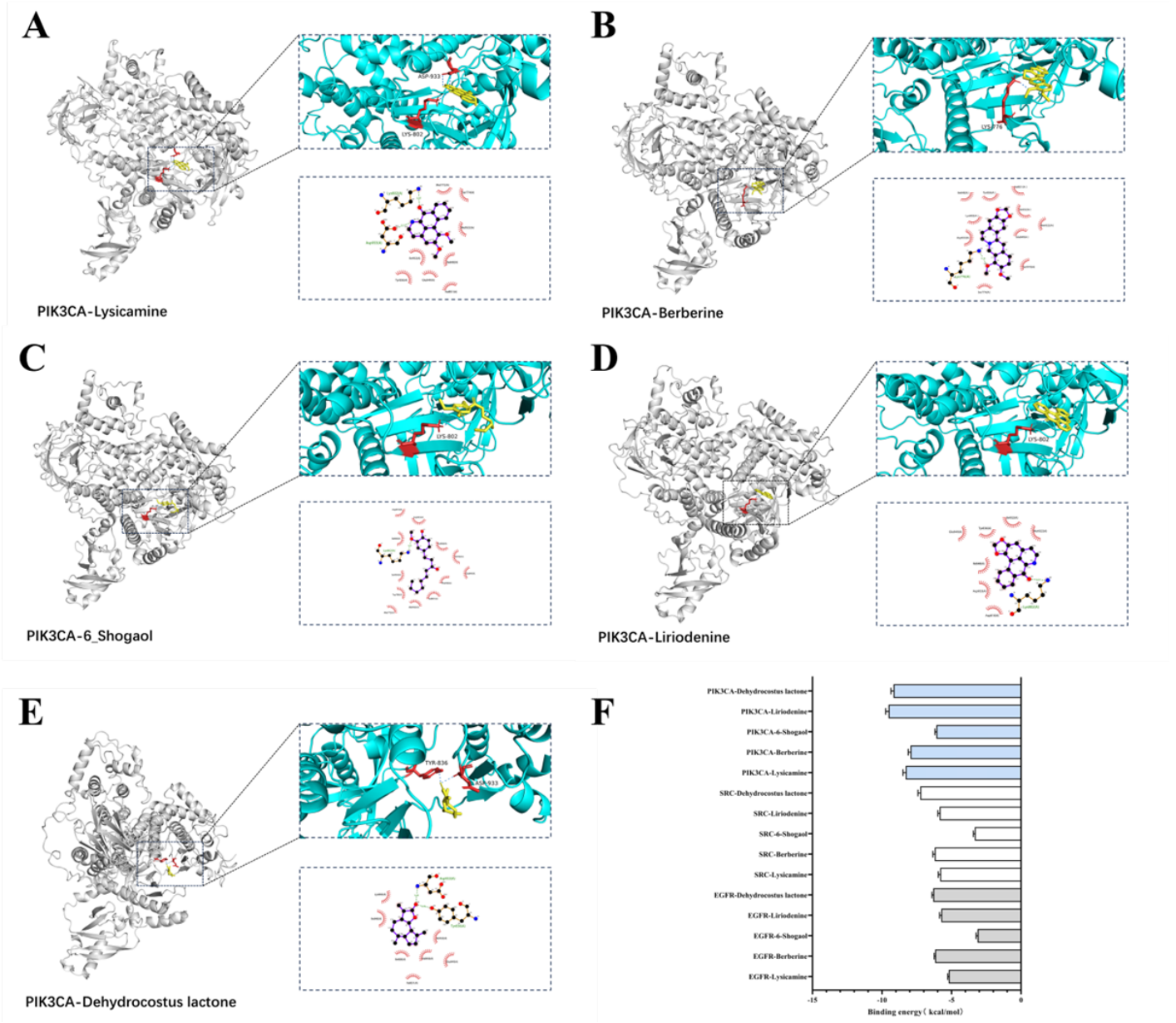

Figure 6: Molecular docking analysis of selected compound–protein systems: predicted three-dimensional binding poses and two-dimensional interaction diagrams for PIK3CA with (A) lysicamine, (B) berberine, (C) 6-shogaol, (D) liriodenine, and (E) dehydrocostus lactone; and (F) predicted docking energies for all 15 compound–protein systems. Values in panel F are presented as the mean ± SD in kcal/mol.

a multi-component interpretation is particularly appropriate for an ethanol extract, in which alkaloids, phenolics, terpenoids, and other constituents coexist.

At the same time, the present data do not establish which compound or combination of compounds is responsible for the observed cellular response. The MS-based annotations remain tentative, and quantitative concentrations of the candidate compounds were not determined. Therefore, the candidate compounds should be regarded as hypotheses for further investigation rather than confirmed active principles.

Convergence of candidate compounds with cancer-related signaling networks

The network pharmacology results provide a second level of interpretation by placing the candidate constituents within a broader molecular context. The identification of PIK3CA, SRC, and EGFR as putative hub genes suggests that the predicted targets are concentrated around signaling proteins that occupy central positions in cancer-related regulatory networks. PIK3CA encodes the catalytic subunit of class I phosphoinositide 3-kinase and is closely involved in PI3K/AKT-mediated regulation of cell survival, proliferation, and metabolism. EGFR is a membrane receptor tyrosine kinase capable of activating multiple downstream pathways, including PI3K/AKT and MAPK, whereas SRC functions as a non-receptor tyrosine kinase involved in proliferative, migratory, and invasive signaling. The simultaneous emergence of these three proteins may therefore indicate that the candidate compounds are associated with a signaling network rather than a single isolated molecular event. The convergence of the present computational findings with previous experimental literature is noteworthy. Berberine has been experimentally linked to PI3K/AKT-related signaling in bladder cancer, including 5637 cells, while dehydrocostus lactone has been associated with both PI3K/AKT and MAPK/ERK signaling in other tumor models. Likewise, the reported anticancer activity of 6-shogaol includes modulation of AKT/mTOR-related signaling. Thus, the present network analysis does not merely identify generic cancer-associated genes; rather, several of the predicted pathways overlap with signaling mechanisms previously associated with the biological activities of compounds tentatively detected in the most active extract.

The KEGG enrichment results further support this interpretation. The enrichment of “Pathways in cancer” and “Proteoglycans in cancer,” together with the predominance of kinase-related GO terms, indicates that the overlapping target set is concentrated in molecular processes related to phosphorylation, receptor kinase activity, and cancer-associated signal transduction. This pattern is consistent with the identification of PI3K/AKT- and MAPK-related pathways. Rather than implying activation or inhibition of a specific pathway, the enrichment results indicate that the candidate target set occupies biological networks involved in tumor-cell proliferation, survival, migration, and related processes. Therefore, the enrichment analysis provides a conceptual bridge between the candidate chemical constituents and the observed reduction in MTT-derived cell viability.

The molecular docking results provide further support for prioritizing some of these compound–target relationships. The relatively favorable predicted interactions between several candidate compounds and PIK3CA, particularly liriodenine and dehydrocostus lactone, are consistent with the central position of PIK3CA in the network analysis. However, the agreement among docking, network pharmacology, and literature evidence should be interpreted as convergent hypothesis generation rather than mechanistic confirmation. Docking predicts structural compatibility under a defined computational model; it does not establish that a compound binds the target in cells, changes the target's activity, or produces the observed cellular phenotype through that target.

A possible chemical–biological model for the summer-root extract

Taken together, the results support a preliminary chemical–biological model for the relatively strong activity of the summer-root extract. Organ-dependent metabolism may contribute to the enrichment of particular secondary metabolites in roots collected under the investigated conditions. Among the compounds tentatively detected in the summer-root extract, several have previously been associated with anticancer mechanisms involving apoptosis, cell proliferation, PI3K/AKT, AKT/mTOR, or MAPK-related signaling. The network analysis further identified PIK3CA, SRC, and EGFR as central candidate targets, and the enrichment analysis placed the predicted targets within cancer-related kinase signaling networks. These independent lines of evidence therefore converge on a model in which multiple constituents of the summer-root extract may influence interconnected signaling processes associated with cancer-cell survival and proliferation.

Importantly, this model should be regarded as a working hypothesis rather than a demonstrated mechanism. The current study did not measure pathway activity, phosphorylation of AKT or related proteins, apoptosis, cell-cycle progression, or direct compound–target interactions. Moreover, the MTT assay measures cellular metabolic activity and cannot independently distinguish reduced proliferation from irreversible cell death. Thus, the approximately 83% reduction in MTT-derived viability observed after prolonged treatment should not be interpreted as direct evidence that the extract caused 83% cell death. Further studies using orthogonal viability assays, apoptosis and cell-cycle analyses, pathway-specific protein measurements, and functional target-validation experiments will be needed to determine whether the predicted PI3K/AKT- and MAPK-related mechanisms contribute directly to the observed phenotype.

Implications for the evaluation and utilization of *L. chinense* resources

The findings extend beyond the simple characterization of a bioactive plant extract. The integrated workflow established in this work demonstrates a rational route for exploring botanicals with complex metabolite profiles: starting from cytotoxicity screening, selecting the most potent sample, performing chemical profiling, and finally predicting potential molecular targets and

pathways. This sequential framework helps translate a crude plant extract into concrete, verifiable hypotheses for follow-up mechanistic research. Although the summer-root extract exhibited the strongest antiproliferative effect against 5637 cells in this assay, further translational development should balance bioactivity with practical considerations including extraction yield, marker compound abundance, biomass accessibility, and sustainable harvesting. For *L. chinense*, this summer-root extract is a promising candidate for subsequent research, and the compounds and signaling networks predicted herein offer clear directions for future isolation, validation, and mechanistic validation studies.

Conclusions

This study screened the antiproliferative activity of ethanol extracts from *L. chinense* and selected the summer root extract with the strongest inhibitory effect on 5637 cells for chemical characterization. GC–MS and UPLC–Q-TOF–MS operated in positive-ion mode were combined to characterize its chemical constituents, offering complementary coverage of volatile, semi-volatile and non-volatile metabolites across different polarity ranges.

MTT screening showed that the summer-root extract produced the greatest reduction in human bladder cancer 5637-cell viability, reaching approximately 83% inhibition after 48 h under the tested conditions. Berberine, lysicamine, 6-shogaol, liriodenine, and dehydrocostus lactone were prioritized as candidate constituents. Network pharmacology, functional enrichment analysis, and molecular docking predicted associations between these compounds and putative targets such as PIK3CA, SRC, and EGFR and generated hypotheses involving cancer-related pathways, including PI3K/AKT and MAPK signaling.

Overall, the present work demonstrates that the summer-harvested root extract of *L. chinense* exerts potent antiproliferative activity against 5637 cells, and provides a comprehensive chemical profile of this active sample to support further research. Nevertheless, the observed cellular response cannot yet be attributed to individual constituents, and the UPLC–Q-TOF–MS annotations and predicted compound–target relationships remain provisional. Confirmation using authentic standards, quantitative chemical analysis, bioactivity-guided fractionation, orthogonal cell-viability and cell-death assays, evaluation in additional cancerous and non-malignant urothelial cell models, and experimental validation of the predicted targets and pathways are therefore required.

Author Contributions

Shaojie Qu contributed to manuscript writing, study design, and literature search.

Guanyan Li, Yuanyuan Chen, and Qing Mao contributed to formal analysis.

Wanxi Peng and Xiaochen Yue contributed to writing review and editing.

References

1. Kieu T, Yanase E. From ethnomedicine to molecular networking and beyond: strategy evolution in medicinal plant-based natural-product discovery. Chemistry Letters. 2026; 55: 3.
2. Wu W, Wu H, Liang R, et al. Light regulates the synthesis and accumulation of plant secondary metabolites. Front Plant Sci. 2025; 4: 1644472.
3. He Y, Li K, Wu Y, et al. Lirispirolides A-L, a new class of sesquiterpene-monoterpene heterodimers with anti-neuroinflammatory activity from the rare medicinal plant Liriodendron chinense. Chin J Nat Med. 2025; 23: 938-950.
4. Pan J, Zhang C, Shi M, et al. Ethanol extract of Liriodendron chinense (Hemsl.) Sarg barks attenuates hyperuricemic nephropathy by inhibiting renal fibrosis and inflammation in mice. J Ethnopharmacol. 2021; 10: 113278.
5. Chand J, Fanai H, Ahmad S, et al. Computational Analysis of Liriodenine's Therapeutic Potential in Breast Cancer: Targeting EGFR and the Complex Oncogenic Network for Drug Discovery. Chem Biodivers. 2025; 22: e00885.
6. Liu X, Li K, Chen H, et al. Bioactive polyketides and tryptophol alkaloids from the endophytic fungus Botryosphaeria dothidea LE-07 of Chinese tulip tree. Fitoterapia. 2024; 179: 106229.
7. Bai J, Wang H, Hu Y. Prediction of Potential Suitable Distribution of Liriodendron chinense (Hemsl.) Sarg. in China Based on Future Climate Change Using the Optimized MaxEnt Model. Forests. 2024; 15: 988.
8. Primus P, Wu C, Kao C, et al. A New Oxoaporphine and Liriodenine's Anti-Neuroblastoma Potential from the Roots of Polyalthia bullata King. Sains Malaysiana. 2024; 53: 359-367.
9. Chen Y, Shen J, Yuan M, et al. Dehydrocostus lactone suppresses gastric cancer progression by targeting ACLY to inhibit fatty acid synthesis and autophagic flux. J Adv Res. 2025; 67: 331-348.
10. Wang K, Yin J, Chen J, et al. Inhibition of inflammation by berberine: Molecular mechanism and network pharmacology analysis. Phytomedicine. 2024; 128: 155258.
11. Attallah K, El-Dessouki A, Abd-Elmawla M, et al. The therapeutic potential of naturally occurring 6-shogaol: an updated comprehensive review. Inflammopharmacology. 2025.
12. Okayama M, Matsumoto T, Kitagawa T, et al. Cytotoxic activities of alkaloid constituents from the climbing stems and rhizomes of Sinomenium acutum against cancer stem cells. J Nat Med. 2024; 78: 226-235.
13. Yan Z, Zhou F, Liang J, et al. Distinction and quantification of Panax polysaccharide extracts via attenuated total reflectance-Fourier transform infrared spectroscopy with first-order derivative processing. Spectrochimica Acta Part a-Molecular and Biomolecular Spectroscopy. 2024, 313.
14. Frolova N, Bilova T, Silinskaia S, et al. Gas Chromatography-Mass Spectrometry (GC-MS) in the Plant Metabolomics Toolbox: GC-MS in Multi-Platform Metabolomics and Integrated Multi-Omics Research. Int J Mol Sci. 2026; 27: 1343.

15. Yang J, Han X, Wang H, et al. Comparison of metabolomics of Dendrobium officinale in different habitats by UPLC-Q-TOF-MS. Biochemical Systematics and Ecology. 2020; 89: 104007.
16. Roviello G, Catalano M, Santi R, et al. Immune Checkpoint Inhibitors in Urothelial Bladder Cancer: State of the Art and Future Perspectives. Cancers. 2021; 13: 4411.
17. Bray F, Laversanne M, Sung H, et al. Global cancer statistics 2022: GLOBOCAN estimates of incidence and mortality worldwide for 36 cancers in 185 countries. CA Cancer J Clin. 2024; 74: 229-263.
18. Patwardhan M, Mahendran R. The Bladder Tumor Microenvironment Components That Modulate the Tumor and Impact Therapy. Int J Mol Sci. 2023; 24: 12311.
19. Noor F, Ul Qamar M, Ashfaq U, et al. Network Pharmacology Approach for Medicinal Plants: Review and Assessment. Pharmaceuticals. 2022; 15: 572.
20. Ferreira L, Andricopulo A. ADMET modeling approaches in drug discovery. Drug Discovery Today. 2019; 24: 1157-1165.
21. Ma S, Wang Q, Wang H, et al. Investigation of the mechanism of Bark of Ailanthus altissima in the treatment of ulcerative colitis based on network pharmacology and experimental verification. J Ethnopharmacol. 2025; 337: 118916.
22. Cavalu S, Abdelhamid A, Saber S, et al. Cell cycle machinery in oncology: A comprehensive review of therapeutic targets. FASEB J. 2024; 38: e23734.
23. Tewari D, Patni P, Bishayee A, et al. Natural products targeting the PI3K-Akt-mTOR signaling pathway in cancer: A novel therapeutic strategy. Semin Cancer Biol. 2022; 80: 1-17.
24. Strati A, Adamopoulos C, Kotsantis I, et al. Targeting the PD-1/PD-L1 Signaling Pathway for Cancer Therapy: Focus on Biomarkers. Int J Mol Sci. 2025; 26: 1235.
25. Rubin S, Sage J, Skotheim J. Emerging Strategies to Inhibit the G1/S Transition for Cancer Therapy. Cancer Res. 2026; 86: 1545-1557.
26. Li Q, Qing L, Xu W, et al. Berberine Affects the Proliferation, Migration, Invasion, Cell Cycle, and Apoptosis of Bladder Cancer Cells T24 and 5637 by Down-Regulating the HER2/PI3K/AKT Signaling Pathway. Archivos Españoles de Urología. 2023; 76: 152-160.
27. Gao X, Liu J, Fan D, et al. Berberine enhances gemcitabine-induced cytotoxicity in bladder cancer by downregulating Rad51 expression through inactivating the PI3K/Akt pathway. Oncol Rep. 2022; 47: 10.3892.
28. Lin L, Chen Z, Huang P, et al. Berberine inhibits the malignant cell phenotype by inactivating PI3K/AKT/mTOR signaling in laryngeal squamous cell carcinoma. Histol Histopathol. 2024; 39: 1527-1536.
29. Rahim U, Mustapa M, Shakrin N, et al. Current evidence and future direction on evaluating the anticancer effects of curcumin, gingerols, and shogaols in cervical cancer: A systematic review. PLoS One. 2024; 19: e0314280.
30. Pei X, He Z, Yao H, et al. 6-Shogaol from ginger shows anti-tumor effect in cervical carcinoma via PI3K/Akt/mTOR pathway. Eur J Nutr. 2021; 60: 2781-2793.
31. Wan M, Dai J, Gan A, et al. A network pharmacology approach to investigate dehydrocostus lactone inhibits the proliferation and epithelial-mesenchymal transition of human gastric cancer cells via regulating the PI3K/Akt and extracellular signal-regulated kinases/mitogen-activated protein kinase signalling pathways. Journal of Pharmacy and Pharmacology. 2023; 75: 1344-1356.
32. Yang J, Sun Y, Liang F, et al. Network pharmacology analysis and in vitro experimental validation of liriodenine against non-small cell lung cancer. Bmc Cancer. 2025; 26: 158.
33. Rodrigues M, Michelli A, Caso G, et al. Lysicamine Reduces Protein Kinase B (AKT) Activation and Promotes Necrosis in Anaplastic Thyroid Cancer. Pharmaceuticals. 2023; 16: 1687.

Appendix

Table 1: Molecular docking results showing binding free energies (ΔG, kcal/mol) of selected.

Group	Binding energy
EGFR-Lysicamine	-5.19±0.23
EGFR-Berberine	-6.18±0.27
EGFR-6-Shogaol	-3.02±0.18
EGFR-Liriodenine	-5.7±0.25
EGFR-Dehydrocostus lactone	-6.3±0.29
SRC-Lysicamine	-5.76±0.24
SRC-Berberine	-6.19±0.26
SRC-6-Shogaol	-3.32±0.19
SRC-Liriodenine	-5.87±0.25
SRC-Dehydrocostus lactone	-7.2±0.31
PIK3CA-Lysicamine	-8.2±0.35
PIK3CA-Berberine	-7.9±0.33
PIK3CA-6-Shogaol	-6±0.28
PIK3CA-Liriodenine	-9.5±0.41
PIK3CA-Dehydrocostus lactone	-9.1±0.38

Table 2: GC-MS identified compounds from summer root ethanol extract of Liriodendron chinense: names, relative contents (%) and molecular formulas.

Serial Number	Name	Proportion	Formula
1	Azulene[4,5-b]furan-2(3H)-one, decahydro-3,6,9-tris(methylene)-, [3aS-(3a.alpha.,6a.alpha.,9a.alpha.,9b.beta.)]-	63.733%	$C_{15}H_{18}O_2$
2	2-Naphthalenemethanol, decahydro-. alpha.,. alpha.,4a-trimethyl-8-methylene-, [2R-(2.alpha.,4a.alpha.,8a.beta.)]-	12.523%	$C_{15}H_{26}O$
3	13-Docosenamide, (Z)-	6.561%	$C_{22}H_{43}NO$
4	2(3H)-Benzofuranone, 6-ethenylhexahydro-6-methyl-3-methylene-7-(1-methylethenyl)-, [3aS-(3a.alpha.,6.alpha.,7.beta.,7a.beta.)]-	4.869%	$C_{15}H_{20}O_2$
5	3,7-Cyclodecadiene-1-methanol, α,α,4,8-tetramethyl-, [s-(Z,Z)]	2.307%	$C_{15}H_{26}O$
6	1,5-Cyclodecadiene, 1,5-dimethyl-8-(1-methylethenyl)-, [S-(Z,E)]-	2.176%	$C_{15}H_{24}$
7	1,3,6,10-Cyclotetradecatetraene, 3,7,11-trimethyl-14-(1-methylethyl)-, [S-(E,Z,E,E)]-	1.774%	$C_{20}H_{32}$
8	(E)-2,6-Dimethoxy-4-(prop-1-en-1-yl)phenol	1.624%	$C_{11}H_{14}O_3$
9	Cyclohexene, 3-(1,5-dimethyl-4-hexenyl)-6-methylene-, [S-(R*,S*)]-	1.605%	$C_{15}H_{24}$
10	Heptanoic acid, 2-ethyl-	1.037%	$C_9H_{18}O_2$
11	Bicyclo[5.2.0]nonane, 4-methylene-2,8,8-trimethyl-2-vinyl-	0.935%	$C_{15}H_{24}$
12	1,4-Methanocycloocta[d]pyridazine, 1,4,4a,5,6,9,10,10a-octahydro-11,11-dimethyl-, (1.alpha.,4.alpha.,4a.alpha.,10a.alpha.)-	0.856%	$C_{13}H_{20}N_2$

Table 3: UPLC–Q-TOF–MS (Positive Ion Mode) Tentatively Identified Constituents in Summer Root Ethanol Extract of Liriodendron chinense: Relative Proportions (%) and Molecular Formulas.

Serial Number	Name	Proportion	Formula
1	Azedarachin C	6.160%	$C_{32}H_{42}O_{10}$
2	13-Deoxo-13alpha-acetyloxy-1-deoxynortaxine B	5.457%	$C_{34}H_{47}NO_8$
3	(2,3)-trans-N-(p-Hydroxyphenethyl)ferulamide	4.324%	$C_{18}H_{19}NO_4$
4	1,2-Dihydrotanshiquinone	4.324%	$C_{18}H_{14}O_3$
5	(-)-Acetoxycollinine	3.799%	$C_{22}H_{26}O_6$
6	Cepharamine	3.431%	$C_{19}H_{23}NO_4$
7	11-O-Acetyl haemanthamine	3.272%	$C_{19}H_{21}NO_{52}$
8	Lanuginosine	3.123%	$C_{18}H_{11}NO_4$
9	Fugapavine	3.078%	$C_{18}H_{17}NO_3$
10	25R-Spirost-4-en-3,12-dione	2.259%	$C_{27}H_{38}O_4$
11	2-(3,4-Methylenedioxyphenyl)-3-methyl-5-(2-oxopropyl)benzofuran	2.205%	$C_{19}H_{16}O_4$
12	Stemonine	1.867%	$C_{17}H_{25}NO_4$
13	(+)-Cassythicine	1.848%	$C_{19}H_{19}NO_4$
14	(-)-Caaverine	1.790%	$C_{17}H_{17}N_2O_4$

15	2-Methoxy-4-(3-methoxy-1-propenyl)-phenol	1.649%	$C_{11}H_{14}O_3$
16	Eleganin	1.450%	$C_{22}H_{26}O_9$
17	(-)-Denudatin B	1.440%	$C_{21}H_{24}O_5$
18	N-Nornuciferine	1.423%	$C_{18}H_{19}NO_2$
19	7-(5',6'-Dihydroxy-3',7'-dimethylocta-2',7'-dienyloxy)-coumarin	1.119%	$C_{19}H_{22}O_5$
20	Caudoside	1.102%	$C_{30}H_{44}O_9$
21	2-(2-Phenylethyl)chromone	1.042%	$C_{17}H_{14}O_2$
22	(-)-Guaia-1(10),11-dien-15-al	1.036%	$C_{15}H_{22}O$
23	Desapidinol	1.027%	$C_{11}H_{14}O_4$
24	Cucurbitacin J 2-O-beta-glucopyranoside	1.014%	$C_{36}H_{54}O_{13}$
25	Plaunol E	0.998%	$C_{22}H_{24}O_8$
26	Pterosin G	0.991%	$C_{14}H_{18}O_3$
27	Eupacunin	0.971%	$C_{22}H_{28}O_7$
28	Decoside	0.962%	$C_{30}H_{42}O_8$
29	2,4-Dimethoxybenzaldehyde	0.957%	$C_9H_{10}O_3$
30	6,9-Epoxy-ergosta-7,22-dien-3-ol	0.900%	$C_{28}H_{44}O_2$
31	Nandazurine	0.896%	$C_{19}H_{13}NO_5$
32	Aknadicine	0.888%	$C_{19}H_{23}NO_5$
33	Codeine	0.888%	$C_{18}H_{21}NO_3$
34	Glabredelphinine	0.878%	$C_{22}H_{33}N_2O_6$
35	Thiamine	0.839%	$C_{12}H_{17}N_4O_2S$
36	Anonaine	0.833%	$C_{17}H_{15}NO_2$
37	7-Hydroxy-3,6-bis(tigloyloxy)tropane	0.756%	$C_{18}H_{27}NO_5$
38	Enanderinanin F	0.742%	$C_{22}H_{26}O_7$
39	Gamma-Guanidinobutyric acid	0.718%	$C_5H_{11}N_3O_2$
40	Ankorine	0.689%	$C_{19}H_{29}N_2O_4$
41	Agrimolide-6-O-beta-D-glucopyranoside	0.676%	$C_{24}H_{28}O_{10}$
42	Betaine	0.642%	$C_5H_{11}NO_2$
43	Acetoin	0.638%	$C_4H_8O_2$
44	Celebroside	0.630%	$C_{40}H_{75}N_2O_9$
45	Tribulusamide A	0.597%	$C_{36}H_{36}N_2O_8$
46	6-Methoxy-7-hydroxycoumarin	0.561%	$C_{10}H_8O_4$
47	Chavicine	0.551%	$C_{17}H_{19}NO_3$
48	14alpha-Methyl-5alpha-ergosta-9(11),24(28)-dien-3beta-ol	0.525%	$C_{29}H_{48}O$
49	Clausine F	0.517%	$C_{19}H_{19}NO_3$
50	21-Hydroxy-30-norhopan-22-one	0.517%	$C_{29}H_{48}O_2$
51	(-)-(2S)-6-Methoxy-[2",3":7,8]-furanoflavanone	0.509%	$C_{18}H_{14}O_4$
52	Histamine	0.482%	$C_5H_9N_3$
53	4,4'-Dihydroxydiphenyl methane	0.482%	$C_{13}H_{12}O_2$
54	alpha-Calacorene	0.449%	$C_{15}H_{20}$
55	Lysicamine	0.439%	$C_{18}H_{13}NO_3$
56	(+)-14-Epicorynoline	0.424%	$C_{21}H_{21}NO_5$
57	Prenyl caffeate	0.409%	$C_{14}H_{16}O_4$
58	Phthalic anhydride	0.403%	$C_8H_4O_3$
59	(+/-)-Car-3-ene-2,5-dione	0.394%	$C_{10}H_{12}O_2$
60	4'-O-Methyl piceid	0.383%	$C_{21}H_{24}O_8$
61	Capillone	0.381%	$C_{12}H_{12}O$
62	Cimiside A	0.372%	$C_{35}H_{56}O_{10}$
63	Turraparvin A	0.363%	$C_{28}H_{36}O_7$
64	Clausenamide	0.360%	$C_{18}H_{19}NO_3$
65	Massonivesinol	0.353%	$C_{20}H_{30}O_8$
66	Amarasterone B	0.345%	$C_{30}H_{50}O_7$
67	1,2,9,10-Tetradehydroaristolane	0.323%	$C_{15}H_{22}$
68	Surangin B	0.317%	$C_{29}H_{38}O_7$
69	Ajugalactone	0.317%	$C_{29}H_{40}O_8$
70	Dihydrocapsacin	0.315%	$C_{18}H_{29}NO_3$

71	L-3alpha,6beta-Ditigloyloxytropane	0.315%	$C_{18}H_{27}NO_4$
72	Coumarinic acid	0.313%	$C_9H_8O_3$
73	Fargesone A	0.311%	$C_{21}H_{24}O_6$
74	10-Hydroxyacetylbaccatin VI	0.307%	$C_{37}H_{46}O_{15}$
75	alpha-Carotene	0.293%	$C_{40}H_{56}$
76	3β-Hydroxy-atractylone	0.284%	$C_{15}H_{20}O_2$
77	Asclepin	0.274%	$C_{31}H_{42}O_{10}$
78	Terpenoid EA-1	0.269%	$C_{30}H_{40}O_8$
79	Dehydrocorydalmine	0.269%	$C_{20}H_{20}NO_4$
80	(-)-3,4-Di-epi-3,7-trifara-9,14-diene	0.268%	$C_{15}H_{24}$
81	Bassianin	0.254%	$C_{23}H_{25}NO_5$
82	Acetylcephalotaxine	0.252%	$C_{20}H_{23}NO_5$
83	Floridinine	0.251%	$C_{15}H_{27}NO_5$
84	10alpha-H-Furanoligularenone	0.251%	$C_{15}H_{18}O_2$
85	Taxezopidine K	0.250%	$C_{37}H_{46}O_{12}$
86	6-Paradol	0.245%	$C_{17}H_{26}O_3$
87	Aschantin	0.241%	$C_{22}H_{24}O_7$
88	Terrestriamide	0.240%	$C_{18}H_{17}N_2O_5$
89	Dihydrocucurbitacin F	0.240%	$C_{30}H_{48}O_7$
90	Thalidomide	0.240%	$C_{13}H_{10}N_2O_4$
91	7-O-Acetyltaxine A	0.240%	$C_{37}H_{49}N_2O_{11}$
92	Boldine	0.234%	$C_{19}H_{21}NO_4$
93	Berberine	0.232%	$C_{20}H_{18}NO_4$
94	Bufalin-3-hydrogen suberate	0.230%	$C_{30}H_{42}O_7$
95	Tetrahydrocorysamine	0.227%	$C_{20}H_{19}NO_4$
96	Fetidine	0.225%	$C_{40}H_{46}N_2O_8$
97	Kupitengester 2	0.217%	$C_{32}H_{37}N_2O_9$
98	6alpha-Methyl-2,6beta-dihydroxymethylbicyclo[3.1.1]-hept-2-ene-2beta-O-glucoside	0.216%	$C_{16}H_{26}O_7$
99	2-Methyl-5-carboxymethyl-7-hydroxychromanone	0.213%	$C_{12}H_{12}O_5$
100	3alpha-Hydroxy-6-oxo-5alpha-cholanic acid	0.208%	$C_{24}H_{38}O_4$
101	Ormosanine	0.207%	$C_{20}H_{35}N_3$
102	Nobilonine	0.206%	$C_{17}H_{27}NO_3$
103	Cocsulinine	0.205%	$C_{35}H_{34}N_2O_6$
104	Chelidonine	0.202%	$C_{20}H_{19}N_2O_5$
105	Schinifoline	0.202%	$C_{17}H_{23}NO$
106	3'-Isobutyryloxy-O-acetyl-2',3'-dihydro-oroselol	0.200%	$C_{20}H_{22}O_7$
107	6-Dehydrogingerdione	0.200%	$C_{17}H_{22}O_4$
108	10beta,14-Dihydroxy-10(14),11beta(13)-tetrahydro-8,9-didehydro-3-deoxyzaluzanin C 10-O-beta-glucopyranosyl	0.200%	$C_{21}H_{30}O_9$
109	6-Shogaol	0.193%	$C_{17}H_{24}O_3$
110	(24S)-Ethylcholesta-5,22,25-trans-3β-ol	0.192%	$C_{29}H_{46}O$
111	Uscharidin	0.191%	$C_{29}H_{38}O_{10}$
112	10-(beta-Hydroxybutyryl)-10-deacetylbaccatin I	0.189%	$C_{33}H_{42}O_{12}$
113	1,3,5,6-Tetrahydroxy-4-phenylxanthone	0.189%	$C_{18}H_{16}O_6$
114	4'-Prenyloxyresveratrol	0.187%	$C_{19}H_{20}O_4$
115	(+)-gamma-Hydroxy-L-homosarginine	0.186%	$C_7H_{16}N_4O_3$
116	Desmodilactone	0.184%	$C_8H_{13}NO_3$
117	Taxuspine H	0.183%	$C_{37}H_{49}NO_9$
118	Liriodenine	0.170%	$C_{17}H_9NO_3$
119	(-)-Olivil	0.167%	$C_{20}H_{24}O_7$
120	Atropine	0.159%	$C_{17}H_{23}NO_3$
121	Anolobine	0.156%	$C_{17}H_{15}NO_3$
122	Aucubigenin	0.155%	$C_9H_{12}O_4$
123	Armillaripin	0.155%	$C_{24}H_{30}O_6$
124	(-)-2β-Hydroperoxykolavelool	0.152%	$C_{20}H_{34}O_3$

125	Chavicol	0.150%	$C_9H_{10}O$
126	Baimuxinfuranic acid	0.148%	$C_{15}H_{24}O_3$
127	(Z,Z,Z)-9,12,15-Octadecatrienoic acid	0.147%	$C_{18}H_{30}O_2$
128	Sinomontanine E	0.142%	$C_{22}H_{35}NO_7$
129	Oxysanguinarine	0.142%	$C_{20}H_{13}NO_5$
130	Malkanguniol	0.140%	$C_{15}H_{26}O_5$
131	3β-Methoxy-9β,19-cyclolanost-23(E)-en-25,26-diol	0.135%	$C_{31}H_{52}O_3$
132	Dehydro-gamma-sanshool	0.134%	$C_{18}H_{25}NO$
133	4-Methyl-7-ergosta-8,24(28)-diene	0.131%	$C_{29}H_{48}$
134	Aromoline	0.130%	$C_{36}H_{38}N_2O_6$
135	Lotusine	0.128%	$C_{19}H_{24}NO_3$
136	Aspidoside A	0.126%	$C_{33}H_{52}O_{12}$
137	6-O-Methyxypiperidin-2-one	0.126%	$C_6H_{11}NO_2$
138	3-(alpha,4-Dihydroxy-3-methoxybenzyl)-4-(hydroxy-3-methoxybenzyl) tetrahydrofuran	0.124%	$C_{20}H_{24}O_6$
139	4-Methyl salicylaldehyde	0.124%	$C_8H_8O_2$
140	Isocanthyline	0.122%	$C_{11}H_{13}NO_3$
141	Tanshilactone	0.111%	$C_{17}H_{12}O_3$
142	Caesalmin A	0.111%	$C_{22}H_{28}O_8$
143	Dibutyl phthalate	0.108%	$C_{16}H_{22}O_4$
144	3-Epischelhammericine	0.108%	$C_{19}H_{23}NO_3$
145	Integerrimine	0.107%	$C_{18}H_{25}NO_5$
146	Coronarian	0.107%	$C_{12}H_{18}N_2O_{12}$
147	Cordycepin	0.105%	$C_{10}H_{13}N_5O_3$
148	Coronaric acid	0.105%	$C_{18}H_{32}O_3$
149	22,23-Dihydroergosterol	0.105%	$C_{28}H_{46}O$
150	3,5-Dimethyl-4-methoxybenzoic acid	0.101%	$C_{10}H_{12}O_3$
151	Apoatropine	0.100%	$C_{17}H_{21}NO_2$
152	4'-Hydroxy-2,6-dimethoxydihydrochalcone	0.099%	$C_{17}H_{18}O_4$
153	Kupitengester 1	0.098%	$C_{34}H_{39}NO_{11}$
154	6-Hydroxy-7-methylesculetin	0.096%	$C_{10}H_8O_3$
155	Precocene	0.096%	$C_{13}H_{16}O_3$
156	Bujeine	0.094%	$C_{20}H_{23}NO_6$
157	Bufarenogin	0.092%	$C_{24}H_{32}O_7$
158	Gentianol	0.090%	$C_{10}H_{11}NO_3$
159	Armillarilin	0.089%	$C_{24}H_{30}O_7$
160	Deoxymorellin	0.085%	$C_{33}H_{38}O_6$
161	6-Methylgingediol	0.085%	$C_{18}H_{30}O_4$
162	Codamine	0.079%	$C_{20}H_{25}NO_4$
163	Mayurone	0.077%	$C_{14}H_{20}O$
164	Coniine	0.072%	$C_8H_{17}N$
165	Kupitengester 4	0.072%	$C_{28}H_{36}O_9$
166	Atractylentrid	0.067%	$C_{14}H_{16}O_3$
167	(Z)-5-Hydroxy-3-butylidene-phthalide	0.065%	$C_{12}H_{12}O_3$
168	Methyl gymnaconitine	0.065%	$C_{35}H_{49}NO_8$
169	Kansuinin B	0.065%	$C_{38}H_{42}O_{14}$
170	Ajugasterone C	0.063%	$C_{27}H_{44}O_7$
171	Tyramine	0.062%	$C_8H_{11}NO$
172	Palustridine	0.061%	$C_{18}H_{31}N_3O_3$
173	Glutinic acid	0.060%	$C_5H_9NO_4$
174	Oxotuberostemonine II	0.054%	$C_{22}H_{31}NO_5$
175	Styrene	0.054%	C_8H_8
176	(+)-Galbacin	0.054%	$C_{20}H_{20}O_5$
177	Filicinic acid	0.053%	$C_8H_{10}O_3$
178	Hypecoumine	0.053%	$C_{19}H_{11}NO_6$
179	Gentianadine	0.053%	$C_8H_7NO_2$

180	Beesioside P	0.052%	$C_{37}H_{62}O_{11}$
181	5alpha-Hydroxy-2alpha-(alpha-methylbutyryl)-oxy-7beta,9alpha,10beta-triacetoxy-4(20),11-taxadiene	0.050%	$C_{31}H_{46}O_9$
182	Irisoquin F	0.048%	$C_{29}H_{50}O_4$
183	Erucic acid	0.046%	$C_{22}H_{42}O_2$
184	1-Phenylhexane	0.045%	$C_{12}H_{18}$
185	Linarionoside A	0.044%	$C_{19}H_{34}O_7$
186	3β,23-Dihydroxy-lup-20(29)-ene-28-O-β-D-glucopyranosyl-(1→6)-β-D-glucopyranoside	0.043%	$C_{40}H_{66}O_{13}$
187	Farnesyl acetate	0.041%	$C_{17}H_{28}O_2$
188	3,8-Dimethoxy-5,7-dihydroxy-3',4'-methylenedioxyflavone	0.041%	$C_{18}H_{14}O_8$
189	2,4-Dihydroxyacetophenone	0.039%	$C_8H_8O_3$
190	Corydalic acid methyl ester	0.038%	$C_{22}H_{23}NO_6$
191	Rhodoxanthin	0.037%	$C_{40}H_{50}O_2$
192	2-Phenyldodecane	0.037%	$C_{18}H_{30}$
193	Hygrine	0.037%	$C_8H_{15}NO$
194	Cucurbitacin C	0.036%	$C_{32}H_{48}O_8$
195	Ecdysterone-22-O-beta-D-glucopyranoside	0.036%	$C_{33}H_{54}O_{12}$
196	Dumoside	0.033%	$C_{40}H_{62}O_{16}$
197	9-Acetoxytaxine B	0.033%	$C_{35}H_{47}NO_9$
198	Taxodine	0.032%	$C_{19}H_{25}NO_3$
199	4-(1,5-Dimethyl-1,4-hexadienyl)-1-methyl-cyclohexene	0.031%	$C_{14}H_{22}$
200	Cassythidine	0.030%	$C_{19}H_{17}NO_5$
201	1,2-Hydronaphthoquinone	0.029%	$C_{10}H_8O_2$
202	Hydrocotarnine	0.029%	$C_{12}H_{15}NO_3$
203	p-Cymene	0.029%	$C_{10}H_{14}$
204	3,3'-Bis(6-methoxychroman)	0.029%	$C_{20}H_{22}O_4$
205	L-Histidine	0.029%	$C_6H_9N_3O_2$
206	(-)-Tetrahydrocoptisine	0.028%	$C_{19}H_{17}N_2O_4$
207	Ponasteroside A	0.027%	$C_{33}H_{54}O_{11}$
208	Bullatine C	0.027%	$C_{26}H_{41}NO_7$
209	Glycozolidal	0.026%	$C_{15}H_{13}NO_3$
210	Carmichaeline	0.026%	$C_{22}H_{35}NO_4$
211	Eseridine	0.025%	$C_{15}H_{21}N_3O_3$
212	Taxuspine S	0.025%	$C_{37}H_{44}O_{14}$
213	3-Hydroxycoumarin	0.025%	$C_9H_6O_3$
214	Ecdysterone-3-O-beta-D-glucopyranoside	0.024%	$C_{32}H_{52}O_{12}$
215	Cannabinol	0.024%	$C_{21}H_{26}O_2$
216	Imidazolylpropionic acid	0.024%	$C_6H_8N_2O_2$
217	Jesaconitine	0.023%	$C_{35}H_{49}NO_{12}$
218	Senkirkine	0.023%	$C_{19}H_{27}NO_6$
219	Tryptophan D1	0.022%	$C_{34}H_{38}O_{10}$
220	Civetone	0.022%	$C_{17}H_{30}O$
221	(22Z,24S)-Cerevisterol	0.021%	$C_{28}H_{46}O_3$
222	14-Benzoyl-8-O-methyl-aconine I	0.021%	$C_{33}H_{47}NO_{10}$
223	Aphylline	0.020%	$C_{15}H_{24}N_2O$
224	Genipinic acid	0.020%	$C_{11}H_{14}O_6$
225	Ergochrysin	0.020%	$C_{31}H_{28}O_{14}$
226	beta-D-Xylopyranosyl-(1→3)-beta-D-xylopyranosyl- (1→4)-alpha-L-rhamnopyranosyl-(1→2)-beta-D-xylo	0.020%	$C_{51}H_{80}O_{20}$
227	Kojic acid	0.020%	$C_6H_6O_4$
228	12alpha-Acetoxyazadironolide	0.019%	$C_{30}H_{38}O_8$
229	1-Acetyl-4-isopropylidene-cyclopentene	0.017%	$C_{10}H_{14}O$
230	Koenigicine	0.017%	$C_{20}H_{21}NO_3$
231	Dictafolin B	0.016%	$C_8H_{10}O_4$
232	Biondnoid I	0.016%	$C_{30}H_{26}O_{13}$

233	Thalicminine	0.016%	$C_{20}H_{15}NO_6$
234	(-)-2beta-Hydroxykolavelool	0.016%	$C_{20}H_{34}O_2$
235	Vomifoliol	0.016%	$C_{13}H_{20}O_3$
236	alpha-Dichroin	0.015%	$C_{16}H_{19}N_3O_3$
237	Cusparine	0.015%	$C_{19}H_{17}NO_3$
238	Berberrubine	0.014%	$C_{19}H_{15}NO_4$
239	6-Hydroxy-eremophilenolide	0.014%	$C_{15}H_{22}O_3$
240	Abyssinone I	0.014%	$C_{20}H_{18}O_4$
241	3,3'-Diacetyl-4,4'-dimethoxy-2,2',6,6'-tetrahydroxy diphenyl methane	0.013%	$C_{19}H_{20}O_8$
242	(-)-Methyl selina-3,11-dien-14-oate	0.013%	$C_{16}H_{24}O_2$
243	1-Methyl-2-nonyl-4(1H)-quinolone	0.012%	$C_{19}H_{27}NO$
244	N-Methylflindersine	0.012%	$C_{15}H_{15}NO_2$
245	Hydroxy-8-(2-hydroxy-3-methylbut-3-enyl)-3,6,7-trimethoxy-2-(3-methylbut-2-enyl)-xanthone	0.011%	$C_{26}H_{30}O_6$
246	Samandarine	0.011%	$C_{19}H_{31}NO_2$
247	(-)-1,10-Epoxy-guaia-11-ene	0.011%	$C_{15}H_{24}O$
248	(3E,7E)-2alpha,10beta-Diacetoxy-5alpha,13alpha,20- trihydroxy-3,8-secotaxa-3,7,11-trien-9-one	0.011%	$C_{24}H_{34}O_8$
249	Brachystamide C	0.010%	$C_{26}H_{37}N_2O_3$
250	Antiarolaldehyde	0.010%	$C_{10}H_{12}O_5$
251	5-Methoxymethyl furfural	0.010%	$C_7H_8O_3$
252	6-alpha-Acetyl-4-O-oxobedfordiaic acid	0.009%	$C_{17}H_{24}O_5$
253	Isopimpinellin	0.009%	$C_{13}H_{10}O_5$
254	5,6-Dimethoxy-7-hydroxycoumarin	0.009%	$C_{11}H_{10}O_5$
255	3-Phenylundecane	0.007%	$C_{17}H_{28}$
256	Caffeic acid	0.007%	$C_9H_8O_4$
257	Chalepensin	0.007%	$C_{16}H_{14}O_3$
258	Lobeline	0.006%	$C_{22}H_{27}N_2O_3$
259	10-Epieupatoroxin	0.006%	$C_{20}H_{24}O_8$
260	Chelerythrine methanolate	0.006%	$C_{22}H_{21}NO_5$
261	1-(4-Hydroxy-3-methoxyphenyl)-3,5-diacetoxyoctane	0.006%	$C_{19}H_{28}O_6$
262	2,6-Dimethoxybenzoquinone	0.005%	$C_8H_8O_4$
263	3,3'-Dimethylquercetin	0.005%	$C_{17}H_{14}O_7$
264	Delavine	0.004%	$C_{27}H_{45}NO_2$
265	Baeckeol	0.004%	$C_{13}H_{18}O_4$
266	Tecostanine	0.003%	$C_{11}H_{21}NO$
267	Isolychnose	0.003%	$C_{24}H_{42}O_{21}$
268	3,4-Teracrylshikonin	0.003%	$C_{23}H_{26}O_6$
269	trans-3-Ethylidene-2-pyrrolidone	0.003%	C_6H_9NO
270	Byak-angelicol	0.003%	$C_{17}H_{16}O_6$
271	Eckol	0.003%	$C_{18}H_{12}O_9$
272	Malvidin	0.002%	$C_{17}H_{15}O_7$
273	Taxuspinanane B	0.002%	$C_{33}H_{40}O_{11}$
274	5,7,2',3'-Tetrahydroxyflavone	0.002%	$C_{15}H_{10}O_6$
275	(Z)-4,5-Dihydro-6,7-cis-dihydroxy-3-butylidene phthalide	0.002%	$C_{12}H_{16}O_4$

© 2026 Shaojie Qu. This article is distributed under the terms of the Creative Commons Attribution 4.0 International License